Organic Electronics 13 (2012) 1401–1408

Contents lists available at SciVerse ScienceDirect

Organic Electronics

journal homepage: www.elsevier.com/locate/orgel

Optimising the efficiency of carbazole co-polymer solar-cells by control over the metal cathode electrode

Darren C. Watters [a], James Kingsley [a,c], Hunan Yi [b], Tao Wang [a], Ahmed Iraqi [b], David Lidzey [a,*]

[a] Department of Physics and Astronomy, The University of Sheffield, Hicks Building, Hounsfield Road, Sheffield S3 7RH, UK
[b] Department of Chemistry, The Dainton Building, University of Sheffield, Sheffield S3 7HF, UK
[c] Ossila Ltd., Kroto Innovation Centre, Broad Lane, Sheffield S3 7HQ, UK

ARTICLE INFO

Article history:
Received 25 January 2012
Received in revised form 21 March 2012
Accepted 23 March 2012
Available online 17 April 2012

Keywords:
Photovoltaic
Fullerene
PCDTBT
Metal oxide
Solar cell
Cathode

ABSTRACT

We have explored the effect of a range of different cathode materials on the power conversion efficiency of organic (polymer) solar cells based on a blend of the conjugated polymer poly[N-9′-heptadecanyl-2,7-carbazole-alt-5,5-(4′,7′-di-2-thienyl-2′,1′,3′-benzothiadiazole)] (PCDTBT) with the fullerene acceptor $PC_{70}BM$. We use a transfer matrix reflectivity model to quantify the optical properties of the cathode and the device structure on its operational efficiency and compare this with the results of experimental measurements. We show that both optical and electrical effects play a role in determining overall device efficiency through their impact on short-circuit current, open circuit voltage and fill-factor. We use our model to demonstrate that devices composed of a thin (60–70 nm) active semiconductor layer and a composite cathode composed of a 5 nm thick layer of calcium capped by aluminium combine low optical loss and improved charge extraction and optimised power conversion efficiency.

1. Introduction

Organic photovoltaic devices (OPVs) are currently the subject of intense research interest as they may offer a means of generating renewable energy from sunlight at lower cost than traditional first-generation solar cells. Before this will be possible, it will be however necessary to improve device efficiency and operational lifetime. Rapid progress is now being made; in 2004 OPVs based on a blend of a polythiophene-based polymer with a fullerene acceptor demonstrated a power conversion efficiency (PCE) of greater than 4% [1]. Very recently organic-based devices have been reported having a PCE in excess of 8% [2], with other reports demonstrating a lifetime of 4000 h under simulated solar radiation [3].

Recently, interest has focused on fabricating solar-cells utilising low energy-gap polymers as the light absorbing and electron donating material combined with an electron-accepting fullerene derivative [4]. One such low energy-gap polymer is the material poly[N-9′-heptadecanyl-2,7-carbazole-alt-5,5-(4′,7′-di-2-thienyl-2′,1′,3′-benzothiadiazole)] (PCDTBT). The extended red-absorption of such materials can lead to improved performance by harvesting a greater fraction of the sun's radiation. Device efficiency is also known to be dependent on the energy-separation between the HOMO level of the donor material and the LUMO level of the acceptor. PCDTBT has a relatively large ionisation potential corresponding to a HOMO level of −5.35 eV [5], leading to OPVs having open circuit voltages in excess of 0.8 V (a value significantly larger than the value of ~0.6 V typically obtained using the polymer poly(3-hexylthiophene) (P3HT)). The larger ionisation potential of PCDTBT also affords the polymer greater air stability as oxidation is suppressed [3,6,7]. When PCDTBT is combined with the electron-accepting fullerene $PC_{70}BM$ in a blend ratio of 1:4 (PCDTBT:$PC_{70}BM$), devices have been fabricated having PCEs of over 7% [8].

* Corresponding author. Tel.: +44 (0) 114 22 23501; fax: +44 (0) 114 22 23555.
E-mail address: d.g.lidzey@sheffield.ac.uk (D. Lidzey).

1566-1199/$ - see front matter © 2012 Elsevier B.V. All rights reserved.
http://dx.doi.org/10.1016/j.orgel.2012.03.039

When cast from solution, PCDTBT forms amorphous films and is therefore characterised by a relatively low hole mobility. To avoid creating OPV devices with low fill-factors (and concomitant charge extraction problems), it has been found necessary to use a relatively thin (<100 nm) PCDTBT:$PC_{70}BM$ layer. However such thin active layers can reduce the effectiveness of optical absorption, and thus optical-interference techniques have been used to maximise the device photocurrent. In particular, a TiO_x cathode interface has been used to improve the photocurrent of P3HT [9] and PCDTBT devices [10], however the deposition of TiO_x on top of the delicate polymer layers requires the use of sol–gel techniques which can necessitate additional thermal treatment processes. An alternative approach to improving the light harvesting capability of PCDTBT:$PC_{70}BM$ OPVs has explored optimising the thickness of the PEDOT:PSS hole extraction layer [11].

Whilst the choice of the semiconducting material used within an OPV is of significant importance in controlling device efficiency, the selection of anode and cathode materials also plays a key role in optimising both optical and electronic properties [12]. A number of authors have explored the role of the OPV cathode in determining efficiency [13–23]. Early work on MDMO-PPV/PCBM heterojunctions [13] demonstrated that the open circuit voltage (V_{oc}) of an OPV was only weakly dependent on the work-function of the cathode, an effect resulting from charge-transfer and Fermi-level pinning of the fullerene acceptor to the metal work-function. This picture has been refined [12], and for a system forming ohmic contacts, the Fermi level of the cathode is pinned to the energy of a negative charge transfer state of the molecular acceptor, while the anode is pinned to the energy of a positive charge-transfer state of the molecular donor. For a system in which non-ohmic contacts are formed, no Fermi-level pinning occurs, with the V_{oc} dependent on the work-function difference between anode and cathode adjusted by some scaling factor [12]. Analytical modelling of organic planar heterojunction solar cells [22] has suggested that the V_{oc} should be independent of the work-function of the cathode, however the choice of cathode will determine the distribution of carriers within the device which will affect series resistance and thus fill-factor (*FF*). Indeed, equivalent circuit models of OPV devices [24] demonstrate that *FF* is reduced by both series and shunt-resistance and is directly correlated with V_{oc}. The reflectivity of the device cathode is also important in determining device efficiency, with cathodes that have higher optical reflectivity (or lower optical loss) resulting in improved energy harvesting capabilities [9,17].

A range of anode materials has been explored to improve device efficiency. In particular metal oxides (such as molybdenum oxide, zinc oxide, nickel oxide, tungsten oxide and titanium oxide) have already been used in OPV devices to create devices having efficiencies between 5% and 7% [7,10,25–27]. The replacement of PEDOT:PSS with a metal oxide anode can result in enhanced charge extraction and the formation of an improved ohmic contact as the work function of such metal oxides is often larger than that of PEDOT:PSS which is between −4.8 and 5.2 eV [28]. For example, in an OPV based on PCDTBT, molybdenum oxide (MoO_3) [27] has proved to be a particularly suitable anode material, as the work function of MoO_3 (around −5.6 eV) forms an ohmic contact with the HOMO level of PCDTBT (located at −5.35 eV). It has also been shown that metal oxide anode materials have additional advantages over PEDOT:PSS; for example, PEDOT:PSS is known to absorb moisture from air which then undergoes a migration into the active layer, therefore decreasing device performance over time [29].

The introduction of such buffer layers within an OPV either at the anode or cathode contact, can cause a redistribution of the electromagnetic field within the active layer. Transfer matrix models provide a useful tool to determine the distribution of the electromagnetic field within such multilayer films and thus can be used to determine the optimum thickness of each individual layer to maximise light harvesting efficiency. Optical models have been applied to a variety of polymer: fullerene systems including those based on MDMO-PPV [30–32], MEH-PPV [33], P3HT [34–35], and in OPV devices incorporating various interface layers [36] such as TiO_x [37–38], ZnO [39] and MoO_3 [27].

In this paper we explore OPV devices utilising a PCDTBT:$PC_{70}BM$ bulk heterojunction active layer and molybdenum oxide (MoO_3) anode extraction layer with a range of different cathode materials. Previous studies have shown that V_{oc} is maximised when lower work-function metals are used as an OPV cathode, [13,15,16,18] as Fermi-pinning results in efficient electron extraction, however metals like calcium suffer from low optical reflectivity and can result in less efficient devices [9,17]. We have therefore explored the use of composite cathode structures based on an optically-thin calcium layer backed by a highly reflective metallic film with the organic semiconductor system PCDTBT:$PC_{70}BM$. We show that this approach leads to device structures having optimised *FF*, V_{oc} and J_{sc}. We also use a transfer matrix model to optimise the optical structure of PCDTBT:$PC_{70}BM$ OPVs for efficient operation, and demonstrate that devices using a composite cathode based on a thin (5 nm) Ca film backed with an optically thick Al layer, combined with a semiconductor layer having a thickness of <100 nm, have a maximum PCE of 5.1%. Our work further demonstrates that simultaneous control over optical and electronic properties is important when optimising OPV devices.

2. Experiment

OPV devices were fabricated on pre-patterned ITO electrodes with a resistance of 20 ohm/square provided by Ossila Ltd. The active area of each pixel was 4.5 mm^2, however a calibrated aperture mask having an area of 2.12 mm^2 was used during device measurement to define the extent of the illuminated area. The ITO substrates were first cleaned in an ultrasonic bath using a 10% sodium hydroxide solution for 5 min followed by a further 5 min in IPA. The substrates were transferred to a vacuum chamber inside a nitrogen-filled glovebox where a MoO_3 anode buffer layer having a thickness between 10 and 40 nm was thermally evaporated at a rate of 0.5 Å s^{-1} onto the ITO substrate. The active semiconductor layer (a 1:4 blend by

weight of PCDTBT:$PC_{70}BM$ at a concentration of 20 mg/ml) was then spun onto the MoO_3 from chlorobenzene forming a film that was between 50 and 100 nm thick depending on the spin-speed. Both organic semiconductor materials were provided by Ossila Ltd and were used without further purification. The PCDTBT was synthesized according to previously described methods [40], and had a molecular weight (M_w) of 32,600 and a polydispersity (PDI) of 1.45.

A cathode was coated onto the PCDTBT:$PC_{70}BM$ layer by thermal evaporation. In each case the chamber base-pressure on evaporation was less than 1×10^{-6} mbar. A number of metals and combinations of metals were explored as cathode materials, including silver, aluminium, calcium, calcium/silver and calcium/aluminium (Ag, Al, Ca, Ca/Ag and Ca/Al respectively). For composite cathodes comprising of Ca backed with a second metal, the thickness of the Ca was fixed at 5 nm whilst the Ag and Al layers were 100 nm. Devices were then encapsulated under nitrogen using a UV epoxy and glass slide. Measurements were conducted in air using a Newport 92251A-1000 AM1.5 solar simulator with NREL certified silicon reference cell and a Keithley 237 sourcemeter.

Optical modelling was performed on a range of test structures using a transfer matrix (TM) reflectivity model [41] that is freely available. As input into the model, the real (n) and imaginary (k) parts of the refractive index for glass, ITO, Ag, Al and Ca as a function of wavelength were taken from an associated program library. The optical constants of thin-films of a PCTDBT:$PC_{70}BM$ (1:4) blend and MoO_3 were determined using spectroscopic ellipsometry; the result of which are shown in Fig. 1(a) and (b) respectively. Here, measurements were made over a wavelength range of 375–1000 nm using a spectroscopic ellipsometer (M2000v, J.A. Woollam Co., USA), with PCDTBT:$PC_{70}BM$ (1:4) and MoO_3 films having a thickness of 70 nm and 20 nm respectively, with all samples deposited on a silicon substrate coated with 100 nm of silicon oxide. Values of n and k were extracted from ellipsometry measurements following our previous reported methods [42], using a B-Spline model incorporating a Kramers–Kronig model, over the range 370–800 nm, at a resolution of 0.15 eV.

Using the TM model we are able to predict the optical absorption of each of the individual layers in a device as a function of wavelength, λ. To calculate the maximum possible photocurrent that could be produced by a particular device, we use the wavelength-dependent optical absorption in the active semiconductor layer $A(\lambda)$ determined using the TM model, and then express the maximum photocurrent (J_{max}) using

$$J_{max} = \int_{\lambda_1}^{\lambda_2} \frac{eA(\lambda)I(\lambda)}{hc}\lambda d\lambda. \quad (1)$$

Here $I(\lambda)$ is the AM1.5 solar spectrum, e is the elementary charge, h is Planck's constant and c is the speed of light. The integral limits used in our calculation are $\lambda_1 = 380$ nm and $\lambda_2 = 700$ nm, corresponding to the short-wavelength edge of the solar spectrum when transmitted through glass and the long-wavelength absorption edge of a PCDTBT:$PC_{70}BM$ thin-film blend respectively. In the following analysis, we directly compare J_{max} determined using equation 1, with the short-circuit photocurrent (J_{sc}) from an OPV. Clearly this is a simplification as this comparison ignores losses within the device arising from either geminate or non-geminate recombination. As we show however, this approach permits a number of optical properties of the various OPV devices to be understood.

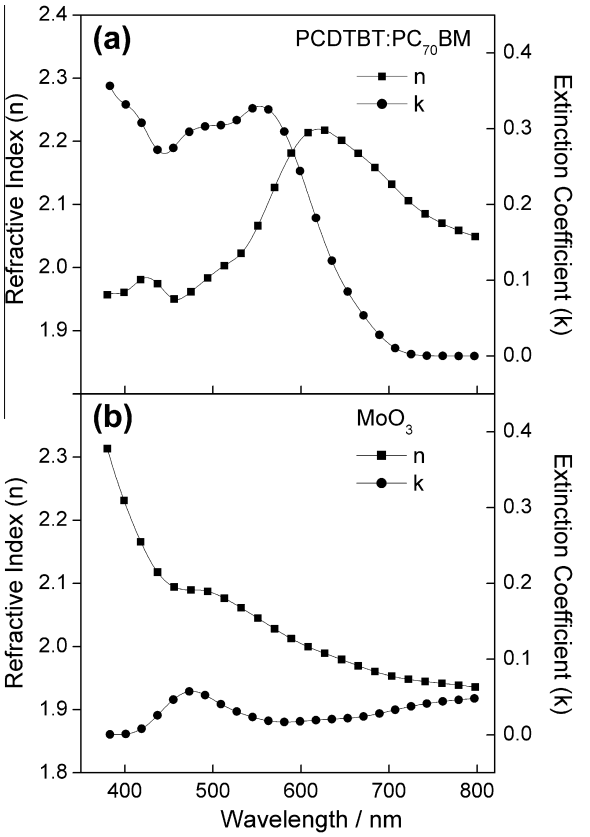

Fig. 1. Refractive index (n) and extinction coefficient (k) for a PCDTBT:$PC_{70}BM$ (1:4) thin-film blend (part (a)) and for a MoO_3 thin film (part (b)).

3. Results and discussion

Fig. 2(a) shows the modelled value of J_{max} for a PCDTBT:$PC_{70}BM$ OPV using an Ag cathode and a 10 nm thick MoO_3 hole extraction layer as a function of the thickness of the PCDTBT:$PC_{70}BM$ layer. It can be seen that there are two maxima in the predicted photocurrent response of the OPV that occur for PCDTBT:$PC_{70}BM$ layer thicknesses of ~70 nm and ~200 nm. These resonances result from optical interference effects within the devices as has been previously demonstrated in OPVs [11,39,43]. It can be seen that the predicted maximum photocurrent for the 200 nm thick PCDTBT:$PC_{70}BM$ layer is 15 mA/cm^2; a value larger than that predicted for an active semiconductor thickness of 70 nm (11.9 mA/cm^2). The larger predicted value of J_{max} anticipated in devices with thicker active layers results directly from the improved optical

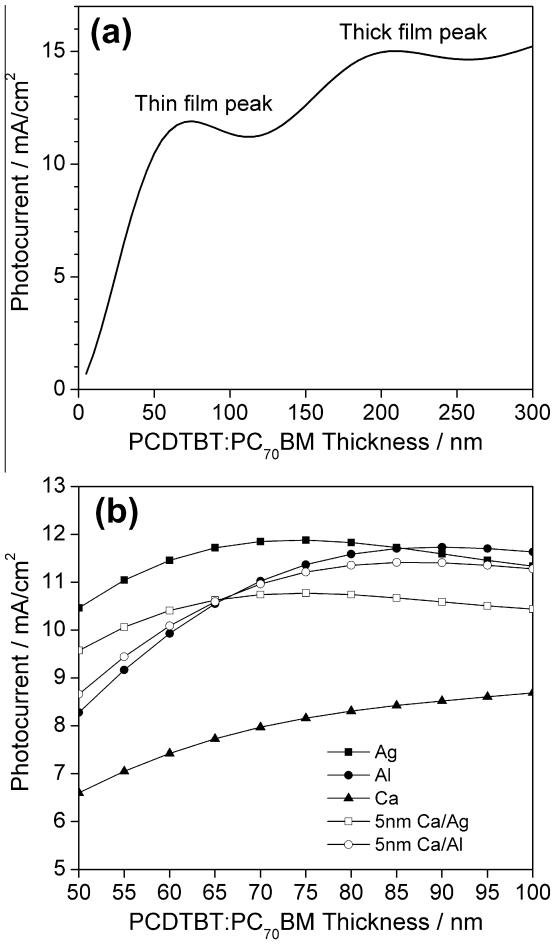

Fig. 2. Part (a) shows modelled photocurrent across a wide range of active layer thicknesses showing the thin and thick film interference peaks. Part (b) shows the modelled photocurrent at the thin film interference peak for a variety of cathodes.

absorption that occurs in more optically dense films. It is clear however that these values most probably over-estimate photocurrent yield as the calculation does not include sub-optimal charge extraction efficiency. We anticipate that as a result of relatively low hole carrier mobility in amorphous polymers such as PCDTBT, efficient charge extraction will be particularly problematic in devices utilising a 200 nm thick PCDTBT:PC_{70}BM film [44]. Indeed, recent spectroscopic studies have indicated that non-geminate recombination and thus incomplete charge-extraction is a dominant loss mechanism in PCDTBT:PCBM OPVs [45]. Furthermore, we note that practical difficulties also arise in producing such thick active layers resulting from the relatively low solubility of PCDTBT [5]. As such we focus the remainder of our studies on OPVs having active layer thicknesses that are less than 100 nm.

In Fig. 2(b), we plot the calculated value of J_{max} from PCDTBT:PC_{70}BM OPV devices utilising either an Ag, Al, Ca, Ca/Ag or Ca/Al cathode as a function of PCDTBT:PC_{70}BM film thickness. We again fix the MoO_3 film thickness at 10 nm. It can be seen that J_{max} is predicted to be a strong function of cathode composition, with high-reflectivity Ag producing devices with the highest overall photocurrent for PCDTBT:PC_{70}BM film thickness less than 85 nm. We note however that for active layer thicknesses greater than 85 nm, a larger photocurrent is predicted from an OPV utilising an Al cathode. It is clear that calcium-based cathodes result in the lowest predicted photocurrents due to its lower reflectivity and greater optical loss. We also plot the predicted photocurrent produced by an OPV with an Ag and Al cathode having a 5 nm Ca interface layer, as has been previously used to create high efficiency OPVs [12]. It can be seen that the incorporation of a thin Ca film appears to have a more significant effect on the photocurrent generated by an Ag cathode compared to an Al cathode. Indeed, the maximum predicted photocurrent that can be generated using a Ca/Ag cathode is around 0.90 times of that which can be generated using an Ag cathode whereas the maximum photocurrent that can be generated using a Ca/Al cathode is around 0.98 times of a regular Al cathode. In the following section, we explore the reasons for the larger predicted reduction in maximum photocurrent that can be generated when a thin Ca layer is placed into an OPV that utilises an Ag cathode.

The analysis presented in Fig. 2 confirms that the optical properties of the cathode play an important role in determining the maximum available photocurrent yield from OPVs containing a relatively thin active organic-semiconductor layer. However, this analysis ignores the effect of the metal work-function on extraction or effects resulting from recombination at an interface, with such effects known to be particularly problematic in OPVs utilising silver, gold or palladium cathodes [12]. The metal Ca is known to efficiently extract electrons in BHJ OPVs utilising fullerene acceptors [9], however the analysis presented in Fig. 2 confirms previous studies [9,17] that indicate that it can reduce device efficiency through introducing increased absorption losses into the device. We have therefore explored the maximum available photocurrent available from an OPV utilising a film of Ca backed by an optically thick film of either Ag or Al. This is shown in Fig. 3 parts (a) and (b) respectively. Here, we have independently varied the thickness of the MoO_3 between 0 and 50 nm, and the thickness of the Ca between 0 and 50 nm. In each case the thickness of the PCDTBT:PC_{70}BM layer was fixed at the respective interference maximum of 75 nm for Ca/Ag and 85 nm for Ca/Al. It can be seen that for all devices, the photocurrent is apparently reduced as the thickness of the MoO_3 layer increases. Our modelling suggests that this effect has two origins; in MoO_3 layers having a thickness $\leqslant$10 nm, it appears that photocurrent is reduced by additional absorption by the MoO_3 with such absorption being approximately linearly dependent upon MoO_3 thickness. This effect is however relatively small; for example in a device incorporating a 10 nm thick MoO_3 film, the absorption by the MoO_3 is around 3% of that of the PCDTBT:PCBM layer. The effect of thicker MoO_3 layers is however more complicated, as such layers both absorb more light and also redistribute the electromagnetic field within the device in a non-linear fashion [46–47]. This redistribution will in many cases reduce the absorption by the active layer and thereby reduce the device photocur-

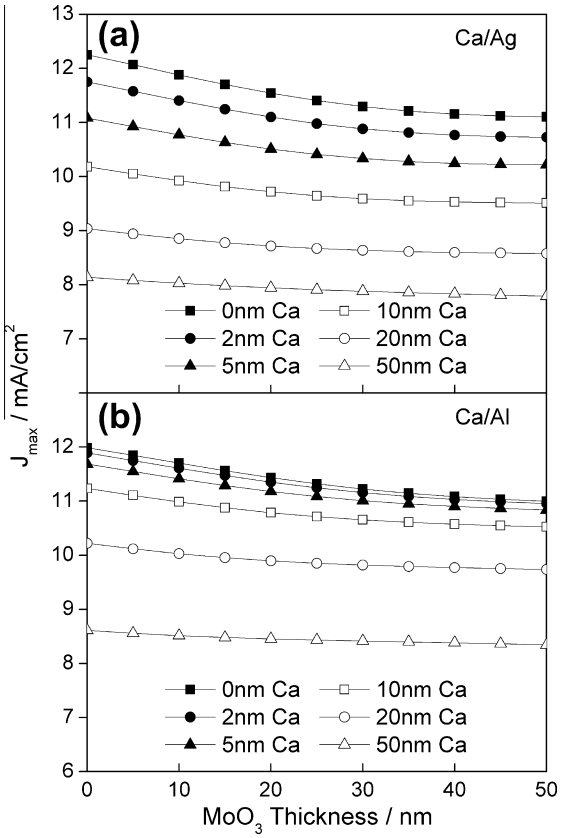

Fig. 3. Part (a) shows the calculated J_{max} for a PCDTBT:$PC_{70}BM$ OPV having a composite Ca/Ag cathode as a function of MoO_3 and Ca layer thicknesses. Here, the thickness of the active semiconductor remains constant at its optimised value of 75 nm. Part (b) similarly shows calculated J_{max} as a function of MoO_3 and Ca layer thicknesses for an OPV device with a Ca/Al cathode for an optimised active semiconductor layer thickness of 85 nm.

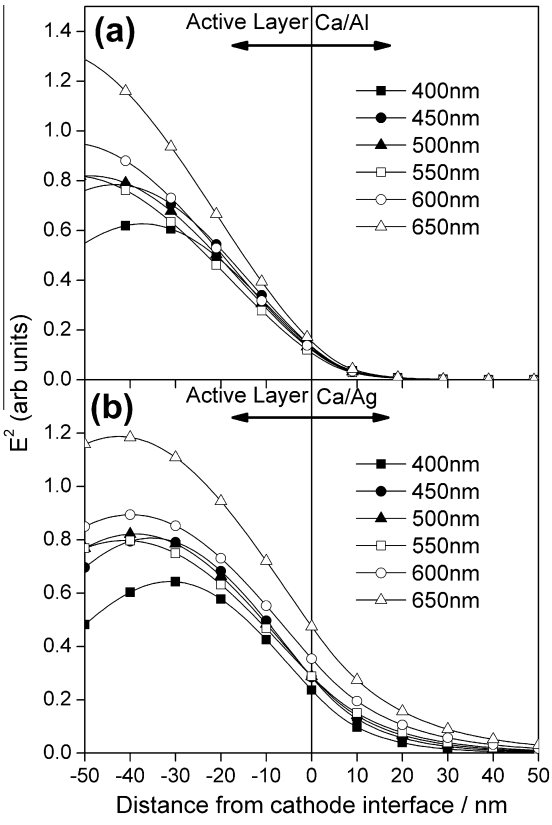

Fig. 4. Part (a) shows the calculated electric field intensity (E^2) at the interface between the active semiconductor layer and the Ca/Al cathode in a PCDTBT:$PC_{70}BM$ OPV. Part (b) similarly shows E^2 for an OPV device utilising a Ca/Ag cathode. In both parts, field intensity is plotted at a number of different characteristic wavelengths as indicated in the figure, with the thickness of the MoO_3 layer constant at 10 nm and the calcium layer being 5 nm.

rent as exemplified by Fig. 3. Our modelling also indicates that the addition of a Ca layer (of any thickness), also reduces J_{max} below that of a device incorporating either a pure Al or Ag cathode. Indeed, we find that greater losses result from the use of thicker Ca layer; a result also consistent with increased optical loss in the absorptive Ca. Intriguingly, our model suggests that the efficiency of Ca interfaces backed with Al are more efficient than those backed with Ag for any given thickness of Ca. This is a surprising result, as it suggests that a composite cathode utilising a Ca film backed by a slightly less reflective Al 'mirror' has lower optical loss than the same Ca film backed by highly reflective Ag.

To explore the origin of this result, we have calculated the optical absorption and field strength within the cathode layers in a composite OPV cathode based on 5 nm of Ca backed with either Al or Ag (as shown in Fig. 4(a) and (b) respectively). The MoO_3 thickness was kept constant at 10 nm and the active layer thickness fixed at 75 or 85 nm (Ca/Ag and Ca/Al respectively). Fig. 4 shows the value of $|E|^2$ (where E is the confined electromagnetic field amplitude within the device) as a function of distance from the cathode interface. Here, data is plotted for a range of wavelengths between 400 and 650 nm. It can be seen that there is a significantly higher penetration of the electromagnetic field into the Ag reflector compared to Al; an effect commensurate with its larger skin-depth (lower optical density). Using our TM model, we are able to calculate the optical absorption within each of the individual layers within the device. In particular, we predict that in a Ca/Ag cathode, the relative total absorption of the optical field in the Ca and Ag layers to be 21% and 4%, respectively. In a device utilising a Ca/Al cathode however, the relative absorption in the Ca and Al layers is 7% and 10% respectively. This demonstrates that whilst Al is more absorptive at optical frequencies than Ag, its smaller skin depth reduces the field intensity close to its surface, and thus absorption in the significantly more absorptive Ca layer is reduced, with more optical energy absorbed by the active semiconductor layer (resulting in a higher value of J_{max} when a composite cathode is used).

To explore the extent to which the optical structure of the cathode determines the practical efficiency of a PCDTBT:$PC_{70}BM$ OPV, we have fabricated a series of devices based on either an Ag, Al, Ca, Ca (5 nm)/Ag or Ca (5 nm)/Al cathode. The *JV* curves of representative devices

are plotted in Fig. 5, with device metrics summarised in Table 1. Note, individual results presented in Table 1 are the average and maximum from at least 24 different pixels with error bars representing the standard deviation about the mean for the top 12 performing pixels. It can be seen that the most efficient devices are created using the Ca/Al composite cathode and have a maximum PCE of 5.0%. We find a small variation in short-circuit current between the different devices, with devices having an Ag cathode displaying the highest values of J_{sc}—a result in qualitative agreement with the modelling results shown in Fig. 2(b). It can be seen however that the J_{sc} recorded from both the composite Ca/Al and Ca/Ag cathode devices are—within experimental uncertainty—identical to one another and also identical to a device using a plain silver cathode. Clearly, the larger photocurrent (approximately 6%) predicted by the use of a Ca/Ag cathode compared to a Ca/Al cathode is not reproduced within experimental uncertainty, however the J_{sc} recorded from devices using a pure Ca cathode are 0.88 times that of the Ag cathode devices – a result qualitatively consistent with enhanced optical loss in the absorptive calcium.

We find that the V_{oc} of the different devices are similar at around 0.85 V; a value consistent with previous studies in which values between 0.75 [44] and 0.91 V [11] have been reported. Interestingly the V_{oc} of devices utilising an Al cathode were significantly lower than those of either Ca or Ag based devices. The reason for this is not understood. It can be seen that despite the work function of the materials used varying by 1.4 eV ($\Phi_{Al} - \Phi_{Ca}$) [13], the differences between the V_{oc} of the different devices do not exceed 100 mV (with only 10 mV separating the V_{oc} of Ag and Ca cathode devices). Notably however, the largest V_{oc} is recorded from devices having a layer of calcium adjacent to the top of the semiconductor surface; an outcome arising from charge transfer to the fullerene and Fermi-pinning [12].

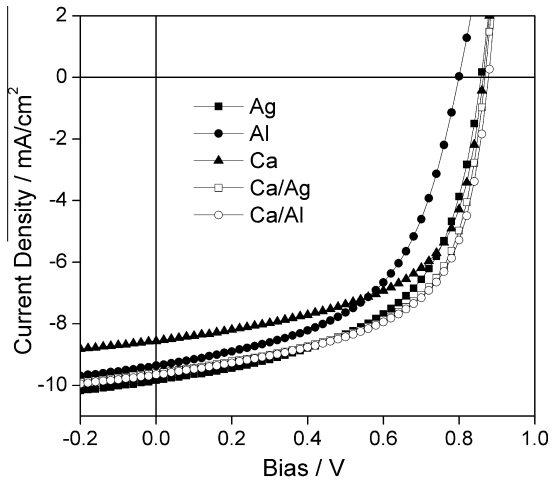

Fig. 5. Measured *JV* curves for Ag, Al, Ca, Ca/Ag and Ca/Al based PCDTBT:$PC_{70}BM$ (1:4) OPV devices having a 10 nm thick MoO_3 hole extraction layer. For both devices utilising a composite cathode, the calcium layer is fixed at 5 nm.

It is clear that there is also a significant difference in the *FF* of the different devices, with largest values of up to 60% being recorded in devices having a Ca/Al cathode. The significantly enhanced *FF* of the Ca/Al, high V_{oc} and relatively high J_{sc} (resulting from low optical loss) result in these devices having the highest *PCE*; a result in agreement with other reports [23] of the effectiveness of composite metal cathodes to optimise the efficiency P3HT:PCBM based devices. Whilst it is difficult to fully account for the origin of the variation in the fill-factor between devices observed here, we note that modelling of planar heterojunction devices indicates that the distribution of charge density within a device is a strong function of the work-function of the metal contact, with low carrier densities at any point within the device leading to high serial resistance [22] and low *FF* [24]. Such models predict that lowest internal resistance is reached when the work-function of the metal contacts are close to the HOMO of the donor or the LUMO of the acceptor [22]. We emphasise however that such models have been specifically developed for planar heterojunction devices and cannot therefore be directly applied to the bulk-heterojunctions studied here. Nevertheless, we note that PCDTBT:$PC_{70}BM$ devices have a strong $PC_{70}BM$ concentration gradient normal to the plane of the device (being $PC_{70}BM$ rich at the surface) [48], and thus such models may provide a first approximation of the solar-cells studied here. More work is clearly necessary to model the role of the metallic cathode workfunction on the charge distribution inside BHJ cells containing graded acceptor concentrations.

Finally, we address the effect of active layer thickness in determining the efficiency of the composite-cathode devices. Here, we have fabricated devices using a composite Ca/Al cathode (5 nm/100 nm) and a 10 nm thick MoO_3 anode buffer-layer. The measured *PCE*, V_{oc} and *FF* of the devices as a function of PCDTBT:$PC_{70}BM$ thickness is shown in Fig 6(a), with the photocurrent (average J_{sc} and J at -1 V) shown in Fig 6(b). For comparison, we also plot J_{max} calculated using the TM model for the device in part (b). As it can be seen, the device V_{oc} remains approximately constant over the range of active layer thicknesses studied (50 to 100 nm). These results are in agreement with other recent studies that also evidenced a drop-off in V_{oc}, *FF* and *PCE* in PCDTBT:$PC_{70}BM$ OPVs as active layer thickness is increased to over 200 nm [44]. We find that the measured value of J_{sc} is on average 15% lower than the predicted J_{max} with the discrepancy between measured and calculated values increasing as the thickness of the active layer increases. When however a bias of –1 V is applied to the device, the agreement between the recorded photocurrent and J_{max} is much improved, although for films having a thickness $\geqslant$80 nm we still find that the recorded photocurrent is slightly less than J_{max}. This clearly indicates that device efficiency is limited by charge extraction; a problem that becomes more severe as active layer thickness increases. This observation is also mirrored in the *FF* that also undergoes some reduction as film thicknesses increases. Indeed, despite the optical model suggesting that the most efficient devices should be created using PCDTBT:$PC_{70}BM$ layer having a thickness of $\sim$85 nm (thereby maximising the short circuit current) we find that the highest device

Table 1
Performance metrics for a series of nominally identical PCDTBT:$PC_{70}BM$ devices prepared using different cathodes.

Cathode	*PCE* average [PCE max] (%)	J_{sc} (mA/cm^2)	V_{OC} (V)	*FF* (%)
Ag	4.55 ± 0.07 [4.68]	9.6 ± 0.1	0.85 ± 0.01	55.7 ± 0.9
Al	3.90 ± 0.06 [4.01]	9.2 ± 0.1	0.78 ± 0.01	53.1 ± 0.9
Ca	4.26 ± 0.04 [4.33]	8.4 ± 0.1	0.86 ± 0.01	58.7 ± 0.4
Ca/Ag	4.81 ± 0.09 [4.94]	9.4 ± 0.2	0.86 ± 0.01	59.5 ± 0.4
Ca/Al	4.90 ± 0.06 [5.01]	9.4 ± 0.1	0.86 ± 0.01	60.6 ± 0.3

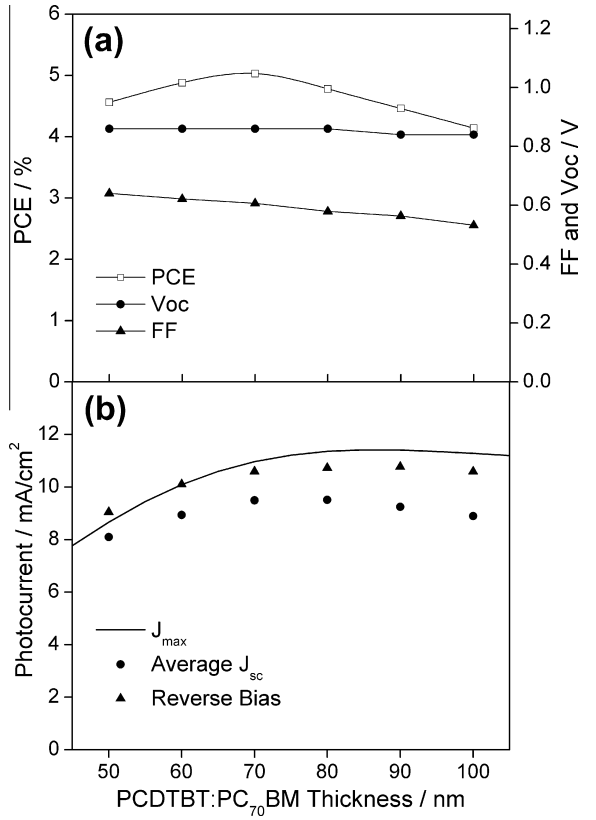

Fig. 6. Part (a) shows the power conversion efficiency (*PCE*), open circuit voltage (V_{oc}) and fill factor (*FF*) of a series of PCDTBT:$PC_{70}BM$ devices having varying active layer thickness, a 10 nm MoO_3 layer and 5 nm Ca buffer layer capped with Al. Connecting lines are used as a guide to the eye. Part (b) shows the measured J_{SC} and photocurrent at a reverse bias of −1 V from a series of OPVs having varying active layer thickness. Also plotted is the predicted maximum photocurrent (J_{max}) of each device calculated using equation 1 (see text for details).

PCE recorded (5.1%) is obtained in devices having a PCDTBT:$PC_{70}BM$ thickness of 70 nm. This confirms other work that suggests that the efficiency of PCDTBT-based OPVs is limited by sub-optimal charge extraction resulting from non-geminate recombination [44]. We note that the efficiencies reported here are smaller than the best reported devices fabricated using PCDTBT:$PC_{70}BM$ blends which have a PCE of 7.1% [8] which have higher values of V_{oc}, *FF* and J_{sc}. Such higher efficiencies were achieved partly through additional solution processing additives and hole-blocking layers to optimise nano-scale morphology and charge extraction.

4. Conclusion

In summary, we have modelled the effects of different cathode structures on the maximum photocurrent that can be generated from a PCDTBT:$PC_{70}BM$ OPV. In particular we focus on composite structures based on a thin film of calcium backed with an optically thick layer of aluminium or silver. We show that device photocurrent is a function of cathode reflectivity, however the work-function of the cathode plays only a minor role in determining device V_{oc} due to Fermi-pinning, but apparently results in devices having improved fill-factor. We show the use of composite cathodes results in both high reflectivity (and thus efficient optical harvesting), good fill factor (efficient charge extraction) and slightly improved open circuit voltage; effects which combine to produce devices having a power conversion efficiency up to 5.1%.

Acknowledgements

We thank the UK EPSRC for funding this work through grants EP/F056370/1 and EP/F016433/1 and for a DTA studentship for DCW. We also thank Andrew J. Pearson for helpful discussions.

References

[1] G. Li, V. Shrotriya, J. Huang, Y. Yao, T. Moriarty, K. Emery, Y. Yang, Nat. Mater. 4 (2005) 864–868.
[2] Z. He, C. Zhong, X. Huang, W.-Y. Wong, H. Wu, L. Chen, S. Su, Y. Cao, Adv. Mater. 23 (2011) 4634–4643.
[3] C.H. Peters, I.T. Sachs-Quitana, J.P. Kastrop, S. Beaupré, M. Leclerc, M.D. McGehee, Adv. Energy Mater. 1 (2011) 491–494.
[4] G. Dennler, M.C. Scharber, C.J. Brabec, Adv. Mater. 21 (2009) 1323–1338.
[5] H. Yi, S. Al-Faifi, A. Iraqi, D.C. Watters, J. Kingsley, D.G. Lidzey, J. Mater. Chem. 21 (2011) 13649.
[6] S. Cho, J.H. Seo, S.H. Park, S. Beaupré, M. Leclerc, A.J. Heeger, Adv. Mater. 22 (2010) 1253–1257.
[7] Y. Sun, J.H. Seo, C.J. Takacs, J. Seifter, A.J. Heeger, Adv. Mater. 23 (2011) 1679–1683.
[8] T.-Y. Chu, S. Alem, S.-W. Tsang, S.-C. Tse, S. Wakim, J. Lu, G. Dennler, D. Waller, R. Gaudiana, Y. Tao, Appl. Phys. Lett. 98 (2011) 253301.
[9] A. Hadipour, D. Cheyns, P. Heremans, B.P. Rand, Adv. Energy Mater. 1 (2011) 930–935.
[10] S.H. Park, A. Roy, S. Beaupré, S. Cho, N. Coates, J.S. Moon, D. Moses, M. Leclerc, K. Lee, A.J. Heeger, Nat. Photonics 3 (2009) 297–303.
[11] T.-Y. Chu, S. Alem, P.G. Verly, S. Wakim, J. Lu, Y. Tao, S. Beaupré, M. Leclerc, F. Bélanger, D. Désilets, S. Rodman, D. Waller, R. Gaudiana, Appl. Phys. Lett. 95 (2009) 063304.
[12] R. Steim, F.R. Kogler, C.J. Brabec, J. Mater. Chem. 20 (2010) 2499–2512.
[13] C.J. Brabec, A. Cravino, D. Meissner, N.S. Sariciftci, T. Fromherz, M.T. Rispens, L. Sanchez, J.C. Hummelen, Adv. Funct. Mater. 11 (2001) 374–380.
[14] C.J. Brabec, A. Cravino, D. Meissner, N.S. Sariciftci, M.T. Rispens, L. Sanchez, J.C. Hummelen, T. Fromherz, Thin Solid Films 403–404 (2002) 368–372.

[15] E. Kymakis, I. Alexandrou, G.A.J. Amaratunga, J. Appl. Phys. 93 (2003) 1764–1768.
[16] C.M. Ramsdale, J.A. Barker, A.C. Arias, J.D. MacKenzie, R.H. Friend, N.C. Greenham, J. Appl. Phys. 92 (2002) 4266–4270.
[17] A.K. Pandey, P.E. Shaw, I.D.W. Samuel, J.M. Nunzi, Appl. Phys. Lett. 94 (2009) 103303.
[18] C. Zhang, S.-W. Tong, C.-Y. Jiang, E.-T. Kang, D.S.H. Chan IEEE Trans. Electron Dev., 57 (2010) 397–405.
[19] V.D. Mihailetchi, P.W.M. Blom, J.C. Hummelen, M.T. Rispens, J. Appl. Phys. 94 (2003) 6849–6854.
[20] V.D. Mihailetchi, L.J.A. Koster, P.W.M. Blom, Appl. Phys. Lett. 85 (2004) 970–972.
[21] Y.S. Eo, H.W. Rhee, B.D. Chin, J.-W. Yu, Synth. Met. 159 (2009) 1910–1913.
[22] D. Cheyns, J. Poortmans, P. Heremans, C. Deibel, S. Verlaak, B.P. Rand, J. Genoe, Phys. Rev. B 77 (2008) 165332.
[23] M.O. Reese, M.S. White, G. Rumbles, D.S. Ginley, S.E. Shaheen, Appl. Phys. Lett. 92 (2008) 053307.
[24] S. Yoo, B. Domercq, B. Kippelen, J. Appl. Phys. 97 (2005) 103706.
[25] M.D. Irwin, D.B. Buchholz, A.W. Hains, R.P.H. Chang, T.J. Marks, Proc. Natl. Acad. Sci. USA 105 (2008) 2783.
[26] T.Y. Chu, S.W. Tsang, J. Zhou, P.G. Verly, J. Lu, S. Beaupre, M. Leclerc, Y. Tao, Sol. Energy Mater. Sol. Cells 96 (2011) 155–159.
[27] Y. Sun, C.J. Takacs, S.R. Cowan, J.H. Seo, X. Gong, A. Roy, A.J. Heeger, Adv. Mater. 23 (2011) 2226–2230.
[28] Y.-J. Lin, F.-M. Yang, C.-Y. Huang, E.-Y. Chou, J. Chang, Y.-C. Lien, Appl. Phys. Lett. 91 (2007) 092127.
[29] E. Voroshazi, B. Verreet, A. Buri, R. Müller, D. Di Nuzzo, P. Heremans, Org. Electron. 12 (2011) 736–744.
[30] H. Hoppe, N. Arnold, N.S. Sariciftci, D. Meissner, Sol. Energy Mater. Sol. Cells 80 (2003) 105–113.
[31] H. Hoppe, N. Arnold, D. Meissner, N.S. Sariciftci, Thin Solid Films 451–452 (2004) 589–592.
[32] J.D. Kotlarski, P.W.M. Blom, L.J.A. Koster, M. Lenes, L.H. Slooff, J. Appl. Phys. 103 (2008) 084502.
[33] D.W. Sievers, V. Shrotriya, Y. Yang, J. Appl. Phys. (2006) 114509.
[34] F. Monestier, J.J. Simon, P. Torchio, L. Escoubas, F. Flory, S. Bailly, R. de Bettignies, S. Guillerez, C. Defranoux, Sol. Energy Mater. Sol. Cells 91 (2007) 405–410.
[35] T. Ameri, G. Dennler, C. Waldauf, P. Denk, K. Forberich, M.C. Scharber, C.J. Brabec, K. Hingerl, J. Appl. Phys. 103 (2008) 084506.
[36] Y. Long, Sol. Energy Mater. Sol. Cells 94 (2010) 744–749.
[37] J.Y. Kim, S.H. Kim, H.-H. Lee, K. Lee, M. Ma, X. Gong, A.J. Heeger, Adv. Mater. 18 (2006) 572–576.
[38] A. Roy, S.H. Park, S. Cowan, M.H. Tong, S. Cho, K. Lee, A.J. Heeger, Appl. Phys. Lett. 95 (2009) 013302.
[39] J. Gilot, I. Barbu, M.M. Wienk, R.A.J. Janssen, Appl. Phys. Lett. 91 (2007) 113520.
[40] N. Blouin, A. Michaud, M. Leclerc, Adv. Mater. 19 (2007) 2295–2300.
[41] G.F. Burkhard, E.T. Hoke, M.D. McGehee, Adv. Mater. 22 (2010) 3293–3297.
[42] T. Wang, A.J. Pearson, D.G. Lidzey, R.A.L. Jones, Adv. Func. Mater. 21 (2011) 1383–1390.
[43] L.H. Slooff, S.C. Veenstra, J.M. Kroon, D.J.D. Moet, J. Sweelssen, M.M. Koetse, Appl. Phys. Lett. 90 (2007) 143506.
[44] Z.M. Beiley, E.T. Hoke, R. Noriega, J. Dacuña, G.F. Burkhard, J.A. Bartelt, A. Salleo, M.F. Toney, M.D. McGehee, Adv. Energy Mater. 1 (2011) 954–962.
[45] F. Etzold, I.A. Howard, R. Mauer, M. Meister, T.-D. Kim, K.-S. Lee, N.S. Baek, F. Laquai, J. Am. Chem. Soc. 133 (2011) 9469–9479.
[46] B.V. Andersson, D.M. Huang, A.J. Moulé, O. Inganäs, Appl. Phys. Lett. 94 (2009) 043302.
[47] R. Steim, F.R. Kogler, C.J. Brabec, J. Mater. Chem. 20 (2010) 2499.
[48] P.A. Staniec, A.J. Parnell, A.D.F. Dunbar, H. Yi, A.J. Pearson, T. Wang, P.E. Hopkinson, C. Kinane, R.M. Dalgliesh, A.M. Donald, A.J. Ryan, A. Iraqi, R.A.L. Jones, D.G. Lidzey, Adv. Energy Mater. 1 (2011) 499–504.